Mineralogical Magazine, December 1999, Vol. 63(6), pp. 813–828

Differential *REE* uptake by sector growth of monazite

G. CRESSEY[1], F. WALL[1] AND B. A. CRESSEY[2]

[1] Department of Mineralogy, The Natural History Museum, Cromwell Road, London SW7 5BD, UK
[2] School of Ocean and Earth Science, Southampton Oceanography Centre, University of Southampton, Southampton SO14 3ZH, UK

ABSTRACT

Monazite-(Ce) from a dolomite carbonatite at Kangankunde, Malawi, is sector-zoned with variation in La_2O_3 of up to 6.0 wt.% and in Nd_2O_3 of up to 3.9 wt.% between sectors. Single crystal X-ray diffraction, backscattered electron imaging and microprobe analysis have been used to establish the relationship between the morphology and sector chemistry of this low-Th monazite, $(Ce,La,Nd)PO_4$. Uptake of La by {011} sector surfaces is enhanced relative to that of $\{\bar{1}01\}$ and {100} sectors; Ce shows no partitioning differences; and uptake of Nd is more easily facilitated on $\{\bar{1}01\}$ and {100} surfaces relative to {011}. There appears to be a distinct relationship between the size of the *REE* ion and the probability of uptake *via* the different growth surfaces. Interpretation of this uptake behaviour, based on theories involving 'protosites', involves an investigation of the possible kink site geometries at edge-steps during growth. Part-formed kink sites with small entrance sizes are calculated to occur with higher frequency on $\{\bar{1}01\}$ relative to {011}, and this correlates with an increase in the smaller-sized *REE* (Nd) uptake by $\{\bar{1}01\}$ growth surfaces. The overall morphology and sector growth is suggested to be a function of uptake chemistry.

KEYWORDS: monazite, sector-zoning, crystal growth, *REE*, carbonatite, Kangankunde.

Introduction

MONAZITE ($(Ce,La,Nd,Th)PO_4$) is a common accessory mineral in many rock types (Overstreet, 1967; Roberts *et al.*, 1990) and, as such, is an important host for rare earth elements (*REE*). It is always enriched in the light *REE* and commonly Ce>La although species are known in which La or Nd predominate as the major *REE* (Clark, 1993). Coupled substitutions involving *REE*, Ca, Th, Si or P in the monazite structure also form solid solutions, leading through to cheralite $(REE,Ca,Th)(P,Si)O_4$ (Burt, 1989). The relationship between the *REE* pattern of the rock-forming fluid or magma and the *REE* uptake behaviour of monazite has a major influence on the whole-rock chemistry. We have studied a low-Th monazite-(Ce) from a carbonatite at Kangankunde, Malawi, in order to examine the crystal chemical controls on the uptake of *REE*.

Rare-earth minerals are common in carbonatites, particularly in rocks that formed late in the sequence of emplacement (Kapustin, 1980; Le Bas, 1989). The Kangankunde carbonatite (35°54′E 13°7′S), in the Chilwa Alkaline Province of Southern Malawi (Woolley, 1991), consists of magnesio- and ferro-carbonatites characteristic of 'late stage' carbonatites. Abundant bright green monazite occurs throughout these carbonatites and also in associated quartz rocks (Garson and Campbell-Smith, 1965; Holt, 1965; Garson, 1966), together with baryte, strontianite, bastnäsite and florencite-goyazite. This assemblage is believed to have been formed by a late stage activity at the magmatic-hydrothermal boundary which was at least partly metasomatic (Wall and Mariano, 1996). In thin section the monazite appears variable in colour from colourless to greenish and brownish, and occurs in aggregates made up of individual euhedral crystals of variable sizes from 20–300 μm. Monazites analysed in 15 rocks from this locality show no obvious relationship between chemistry and colour-variation, and show no distinct variations in composition between different varieties of carbonatite or

between monazite in carbonatites and quartz rocks (Wall and Mariano, 1996). The results reported here are from monazite in two rocks from the Natural History Museum collection: BM1962,73(76), a ferroan dolomite carbonatite in which the monazite occurs as aggregates of 30 μm euhedral crystals with strontianite and baryte in hexagonal, prismatic pseudomorphs after an unknown mineral and BM1962,73(114), in which the monazite occurs as larger, 300 μm crystals in a more coarse grained monazite-baryte-florencite-quartz rock.

Distinct sector zoning of certain *REE* is present in all the monazite crystals from Kangankunde that we have investigated in this study. A structure refinement of monazite from Kangankunde was included in a crystal chemical study of *REE*-phosphates by Ni *et al.* (1995), but these authors appear to have been unaware of the sector zoning in Kangankunde monazite crystals, and therefore it is not certain to which chemical sector(s) their structural data relates.

Analytical techniques

Electron probe microanalysis and element distribution maps were obtained at the Natural History Museum using a Cameca SX50 wavelength-dispersive microprobe operated at 20 kV and 20 nA. Single *REE* calcium aluminium silicate glasses were used as standards for the *REE*, and interferences were removed using empirical correction factors. Backscattered electron imaging was carried out at the University of Southampton using a JEOL JSM 6400 scanning electron microscope with a KE Developments backscattered electron detector and a Tracor Northern Series II energy-dispersive X-ray microanalysis system.

Single-crystal precession X-ray diffraction photographs were recorded at the Natural History Museum using Zr-filtered Mo-$K\alpha$ radiation.

The computer programs ATOMS and SHAPE (Shape Software; Dowty, 1980) were used to model the monazite structure and crystal morphology.

Results

Compositional variations

Compositional variation within single crystals is observed in all monazite at Kangankunde. The form of this chemical variation is not immediately obvious in optical thin section, because it does not correlate with the observed colour variations (green to colourless). However, the compositional variations are revealed by high-contrast backscattered-electron imaging or by element distribution mapping and analysis in the electron microprobe using polished thin sections. Figure 1 shows an example of element distribution maps and associated line scan analyses from typical aggregates of monazite in ferroan dolomite carbonatite at Kangankunde. The main zoning is in La and Nd whereas Ce remains constant. The La_2O_3 values vary from 14 to 25 wt.% and Nd_2O_3 concentrations vary systematically in the opposite sense to La_2O_3, but Ce_2O_3 remains constant at 36–38 wt.%. In common with many other monazites from carbonatites, the Th content is low, usually <0.5 wt.% ThO_2. Strontium is consistently present, typically at the 1–2 wt.% SrO level, but there is no simple relationship between Sr and the changes in *REE* content. It is clear that all the crystals in these aggregates exhibit some kind of sector zoning of La and Nd. However, in this specimen the crystallographic identities and orientations of the sectors are difficult to establish because the crystals are small and intimately intergrown. In order to seek a crystallographic explanation for the monazite sector zoning observed at Kangankunde, crystals from the coarser-grained monazite-quartz rock have been investigated by single-crystal X-ray diffraction.

X-ray diffraction

Two monazite crystals, ~300 μm diameter, each with well-developed morphology, were chosen for single-crystal precession X-ray diffraction experiments from specimen BM1962,73(114). The first crystal proved difficult to orient, because the crystal did not appear to be single; individual crystallites were only slightly misoriented with respect to one another. This whole 'crystal' produced precession photographs with doubled spots in the reciprocal net similar to the effect produced by a single crystal that is slightly misoriented with respect to the X-ray beam direction. The second crystal produced precession photographs with an identical effect of doubled spots, even when the crystal was oriented as close as possible to having x^*z^* and y^*z^* reciprocal lattice sections perpendicular to the beam. These diffraction photographs are shown in Fig. 2. The directions in which doubled spots occur on these

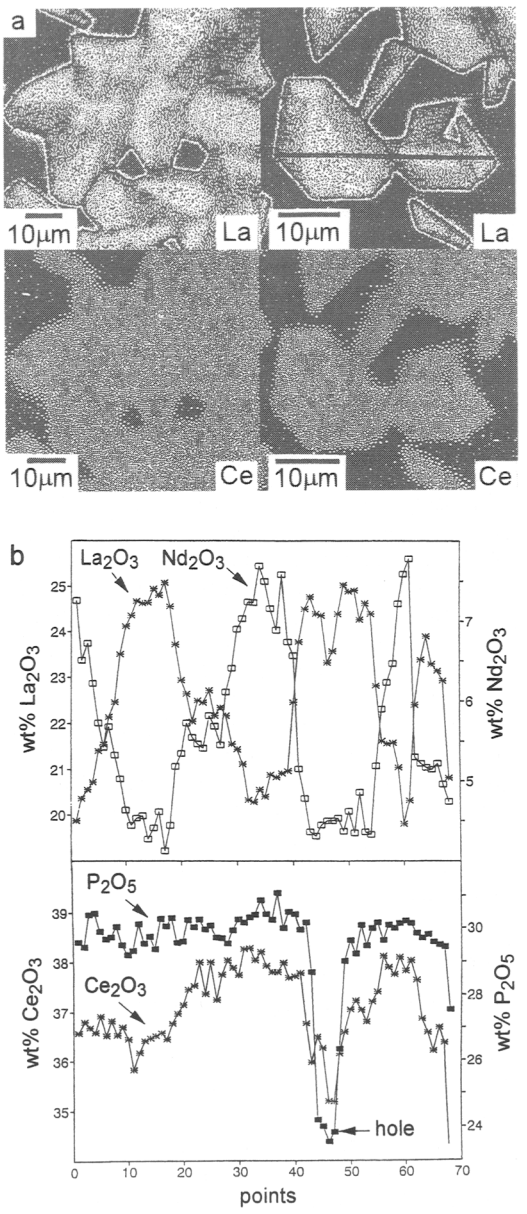

FIG. 1. *a*. EPMA element distribution maps of La and Ce in monazite crystal aggregates from Kangankunde carbonatite sample BM 1962,73(76). Sector zoning is evident from the La distribution. In contrast, the Ce levels are almost constant regardless of sector zone. (*b*) Line-scan point analyses across three sector-zoned crystals (along horizontal line shown on top right map). Sectors high in La are low in Nd and *vice versa*. Levels of P are constant and Ce shows little change.

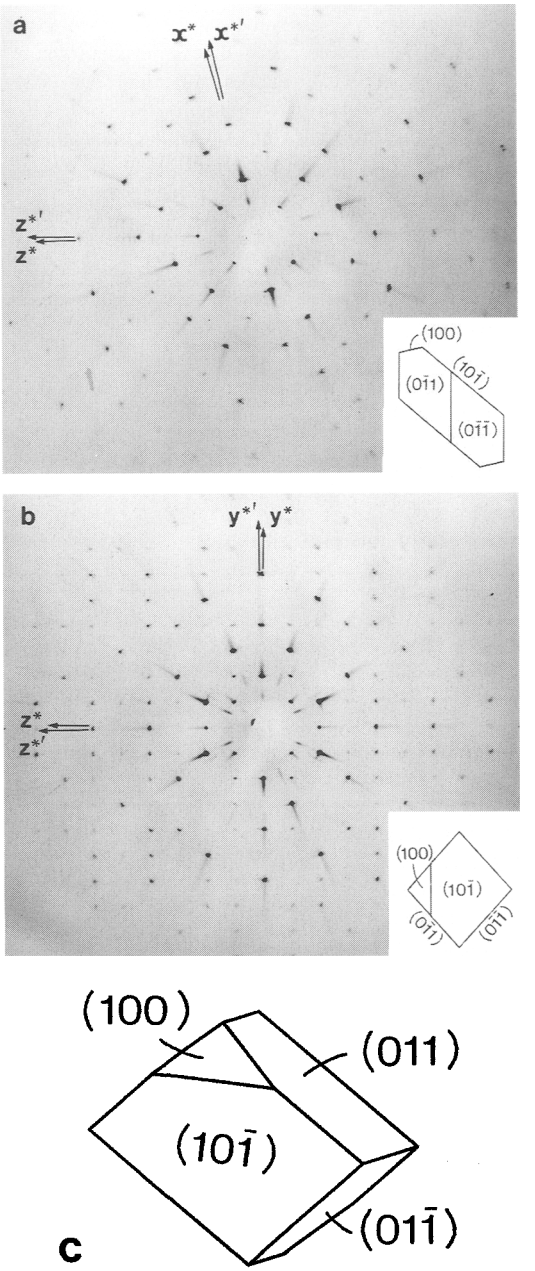

FIG. 2. (*a*, *b*). X-ray precession photographs of monazite from Kangankunde carbonatite sample BM 1962,73(114). The doubled spots indicate a small (~2°) misorientation of the lattice between the chemically-distinct adjacent sectors. Insets show the orientation of the monazite crystal (viewed parallel to the beam direction) for each experiment, and (*c*) shows the flattened $\{\bar{1}01\}$ habit of the 300 μm crystal used.

photographs indicate that there is a relative rotation of the lattice of ~2° about both the x and y axes. This angular misorientation was confirmed by Laue photographs recorded with the crystal stationary, in which reflections appear doubled for the beam parallel to x and y respectively. In addition, Laue photographs taken with the beam perpendicular to $z^*[110]^*$ and $z^*[1\bar{1}0]^*$ planes respectively, both show evidence of tripling of reflections, indicating that a relative lattice misorientation also occurs about the z axis. These results are consistent with the presence of four individual crystals misoriented with respect to one another by ~2°. This misorientation of the lattice is thought to be associated with the sectors in the monazite, and is discussed later.

Morphology and sector growth

A crystallographic description of the monazite crystal morphology has been established directly from the single crystal X-ray diffraction experiments, by observing the morphological orientation of the single crystal with respect to the crystallographic directions in the particular precession photograph produced. Thus determined, the Kangankunde monazite crystal habit is flattened on $\{\bar{1}01\}$, bounded by $\{011\}$, and modified by the small development of $\{100\}$, as shown in Fig. 2*c*. This morphology indicates that the growth rates were faster in directions perpendicular to $\{011\}$ relative to those perpendicular to $\{\bar{1}01\}$ and $\{100\}$; the structural significance of this is discussed later.

The morphological model adopted has been used to determine the crystallographic orientation of monazite crystals seen in only two dimensions in a thin section of the carbonatite rock in which the monazite occurs. A backscattered electron (BSE) image, recorded in the scanning electron microscope, of one such crystal in polished thin section is shown in Fig. 3. Because this is a random section through one monazite crystal, its crystallographic orientation is not immediately obvious. However, by adjusting the relative development of $\{\bar{1}01\}$, $\{011\}$ and $\{100\}$ forms in the model morphology, and constructing a trial series of 2-dimensional sections through the 3-dimensional crystal shape, a solution can be found that matches the outline shape of the crystal observed in the thin section. The result of this exercise is shown in Figs. 4*a* and 4*b*. Thus determined, the 3-dimensional shape of the crystal

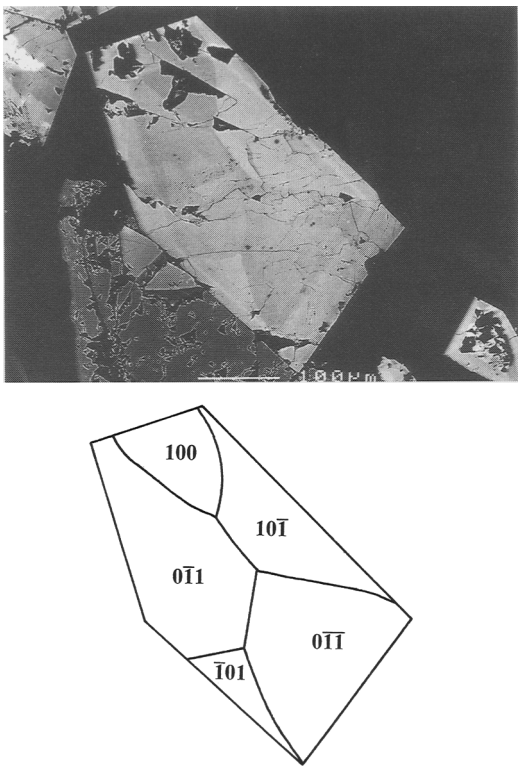

FIG. 3. SEM backscattered electron image of sector-zoned monazite in a monazite-baryte-florencite-quartz rock from Kangankunde, sample BM1962,73(114). The subtly different grey levels reveal the presence of chemically-different sectors; these are outlined in the accompanying sketch with crystallographic indexing of sectors determined from Fig. 4. Chemical analyses of these sectors are given in Table 1; $\{\bar{1}01\}$ sectors are Nd rich, and $\{011\}$ sectors are La rich.

conforming with the observed 2-dimensional section has a very similar morphology to the whole crystal extracted for the X-ray study (Fig. 2), but with a slightly larger development of $\{\bar{1}01\}$ (i.e. flatter) and a slightly larger development of the $\{100\}$ bevel.

Closer inspection of the subtle grey-levels in the BSE image reveals the presence of chemically-different sectors. These sectors can be identified crystallographically from the morphological orientation determined (Fig. 4) and are labelled in the diagrammatic representation in Fig. 3. A 3-dimensional interpretation of the sector growth of the monazite is shown by the stereopair in Fig. 4*c*. The

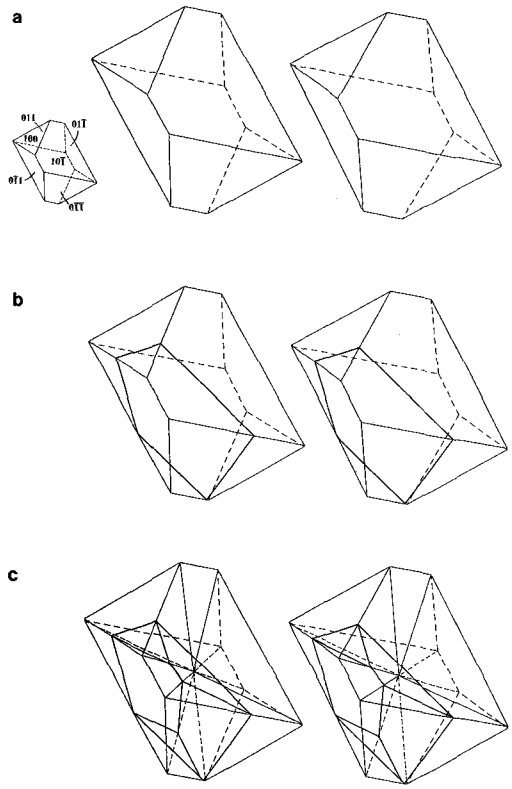

FIG. 4. Stereopairs illustrating the crystallographic orientation of the monazite crystal imaged in thin section (Fig. 3). The cut of the thin section and sector orientations were determined by constructing a series of 2-dimensional slices through a 3-dimensional crystal shape whose relative face sizes were varied whilst maintaining the flattened $\{\bar{1}01\}$ habit observed for monazites in this rock (see Fig. 2). (*a*) final shape that conforms with (*b*) the outline of the crystal observed by the cut of the thin section. (*c*) stereopair showing individual growth sectors and their complex intersection by the thin section. This exercise enables an important link to be made between the chemistry and the crystallography of the sectors.

2-dimensional slice through the crystal intersects several boundaries between the different sectors of the crystal, and these are outlined on the plane constructed through the model crystal. The sector shapes and their boundaries in the plane of the slice constructed through the morphological model closely approximate those observed in the BSE image of the crystal. Therefore, the sectors as outlined in Fig. 4*c* constitute a reasonable model for the domains that were present during the growth of the crystal.

Each sector was built up layer-by-layer from a set of planes parallel to the surfaces (faces) that existed during the growth of the crystal. We describe each growth sector, *hkl*, by the indices of the planes, (*hkl*), that have formed the sector. Eight individual growth sectors are present; these are grouped into four pairs related by a centre of symmetry, and two of these pairs are crystallographically equivalent, as the morphological symmetry is $2/m$. Growth sectors 011, $0\bar{1}\bar{1}$, $0\bar{1}1$ and $01\bar{1}$ are symmetrically (and structurally) equivalent to each other; $\bar{1}01$ and $10\bar{1}$ sectors are also symmetrically related, as are the 100 and $\bar{1}00$ sectors. Therefore, it appears that three crystallographically and structurally distinct types of growth surface were present during the formation of the crystal.

Sector chemistry

The atomic number contrast in the BSE image (Fig. 3) gives a qualitative, but sensitive, assessment of the chemical variation within the monazite crystal. X-ray mapping of this crystal in the SEM indicates that the distribution of La varies between the sector zones. Point analyses from each sector of this crystal have been obtained by wavelength-dispersive electron microprobe analysis (Table 1). From these data it is clear that La is more concentrated in the $\{011\}$ sectors, and lower La concentration is characteristic of both $\{\bar{1}01\}$ and $\{100\}$ sectors. On the other hand, Ce shows no such partitioning; Ce concentration is almost constant for all sectors. The Nd, Pr and the other mid-*REE* are present in higher concentration levels in $\{\bar{1}01\}$ and $\{100\}$ sectors relative to $\{011\}$ sectors; a trend which is the opposite to that shown by La. The lower concentration of La and the higher concentration of Nd in $\{\bar{1}01\}$ and $\{100\}$ sectors explain the relatively higher brightness of the $\{\bar{1}01\}$ sectors in the BSE image, but does not explain the lower brightness level of the $\{100\}$ sector. The analyses show that the Sr level is slightly higher in the $\{100\}$ sector, and this is probably responsible for the lower backscattered intensity in the image. From these data it is clear that the difference in probability of La^{3+} uptake is controlled by the different crystal structural and crystal chemical properties of the surfaces of the growing crystal. For these different surfaces, the probability of La uptake is highest for $\{011\}$ sectors and lowest in

TABLE 1. Electron microprobe analyses of the sector zoned monazite shown in Fig. 3

Sector	$10\bar{1}$		$\bar{1}01$		$0\bar{1}1$ [a]		$0\bar{1}1$ [b]		$0\bar{1}\bar{1}$		100	
n = number of analyses	mean $n = 10$	std. dev.	mean $n = 10$	std. dev.	mean $n = 10$	std. dev.	mean $n = 15$	std. dev.	mean $n = 10$	std. dev.	mean $n = 10$	std. dev.
Al_2O_3	0.03	(0.02)	0.02	(0.02)	0.02	(0.02)	0.06	(0.01)	0.04	(0.05)	0.01	(0.01)
SiO_2	0.17	(0.03)	0.16	(0.04)	0.14	(0.03)	0.17	(0.02)	0.15	(0.03)	0.15	(0.02)
P_2O_5	28.95	(0.51)	29.05	(0.32)	28.57	(0.40)	28.89	(0.33)	28.51	(0.31)	29.48	(0.34)
SO_3	0.24	(0.09)	0.24	(0.11)	0.15	(0.10)	0.12	(0.04)	0.14	(0.09)	0.09	(0.05)
CaO	0.15	(0.03)	0.13	(0.02)	0.16	(0.02)	0.15	(0.04)	0.16	(0.02)	0.19	(0.02)
FeO	0.03	(0.03)	0.04	(0.02)	0.05	(0.04)	0.02	(0.02)	0.03	(0.03)	0.01	(0.02)
SrO	1.28	(0.09)	1.24	(0.16)	1.08	(0.15)	0.98	(0.23)	1.18	(0.11)	1.76	(0.16)
Y_2O_3	0.01	(0.02)	0.04	(0.07)	0.00	(0.00)	0.00	(0.01)	0.00	(0.00)	0.03	(0.06)
La_2O_3	16.06	(0.89)	17.43	(0.68)	22.20	(0.86)	20.09	(0.55)	21.39	(0.64)	17.55	(1.15)
Ce_2O_3	34.52	(0.40)	34.50	(0.34)	34.24	(0.54)	34.31	(0.28)	34.24	(0.39)	34.03	(0.53)
Pr_2O_3	3.38	(0.23)	3.26	(0.14)	2.68	(0.10)	2.89	(0.09)	2.76	(0.14)	3.16	(0.19)
Nd_2O_3	11.53	(0.42)	10.75	(0.45)	7.65	(0.21)	8.45	(0.29)	8.18	(0.34)	10.65	(0.44)
Sm_2O_3	1.34	(0.14)	1.13	(0.08)	0.71	(0.06)	0.83	(0.08)	0.81	(0.07)	1.17	(0.14)
Gd_2O_3	0.41	(0.08)	0.25	(0.09)	0.07	(0.13)	0.31	(0.09)	0.16	(0.08)	0.32	(0.10)
ThO_2	0.33	(0.06)	0.18	(0.10)	0.07	(0.04)	0.12	(0.05)	0.13	(0.07)	0.21	(0.07)
UO_2	0.04	(0.05)	0.02	(0.03)	0.02	(0.04)	0.03	(0.05)	0.02	(0.03)	0.00	(0.00)
Total	98.47		98.44		97.81		97.42		97.90		98.81	

TABLE 1. (*contd.*)

Sector	$10\bar{1}$		$\bar{1}01$		$0\bar{1}1$ [a]		$0\bar{1}1$ [b]		$0\bar{1}\bar{1}$		100	
Atoms per 16 oxygens												
Ca	0.026		0.022		0.028		0.026		0.028		0.032	
Fe	0.004		0.005		0.007		0.003		0.004		0.001	
Sr	0.119		0.115		0.101		0.092		0.111		0.162	
Y	0.001	X_i	0.003	X_i	0.000	X_i	0.000	X_i	0.000	X_i	0.003	X_i
La	0.947	0.242	1.026	0.262	1.323	0.331	1.194	0.303	1.275	0.320	1.027	0.265
Ce	2.021	0.516	2.016	0.514	2.025	0.507	2.024	0.514	2.026	0.508	1.976	0.511
Pr	0.197	0.050	0.190	0.049	0.158	0.040	0.170	0.043	0.163	0.041	0.183	0.047
Nd	0.658	0.168	0.613	0.156	0.441	0.111	0.486	0.124	0.472	0.118	0.603	0.156
Sm	0.074	0.019	0.062	0.016	0.040	0.010	0.046	0.012	0.045	0.011	0.064	0.017
Gd	0.022	0.005	0.013	0.003	0.004	0.001	0.017	0.004	0.009	0.002	0.017	0.004
Th	0.012		0.007		0.003		0.004		0.005		0.008	
U	0.001		0.001		0.001		0.001		0.001		0.000	
Total	4.082		4.073		4.131		4.063		4.139		4.076	
P	3.919		3.926		3.907		3.940		3.901		3.959	
S	0.029		0.029		0.018		0.015		0.017		0.011	
Si	0.027		0.026		0.023		0.027		0.024		0.024	
Al	0.006		0.004		0.004		0.011		0.008		0.002	
Total	3.981		3.985		3.952		3.993		3.950		3.996	
Calculated cell parameters*												
a	6.795		6.797		6.804		6.801		6.802		6.797	
b	7.020		7.023		7.031		7.028		7.029		7.023	
c	6.467		6.469		6.475		6.473		6.474		6.469	
β	103.4		103.4		103.4		103.4		103.4		103.4	

[a] = darker, [b] = lighter intrasectorial zones in backscattered electron image (Fig. 3).
* cell parameters calculated assuming a linear interpolation between end member compositions: $a = \sum_i X_i a_i^0$, where atom fraction $X_i = (REE_i/\sum REE)$
Cell parameters for synthetic end-members $LaPO_4$, $CePO_4$, $PrPO_4$, $NdPO_4$, $SmPO_4$ and $GdPO_4$ taken from JCPDS data sets 32-493, 32-199, 32-885, 25-1065, 32-983 and 32-386 respectively.

{$\bar{1}$01} and {100} sectors, whereas the probability of Ce uptake is essentially constant. However, the partitioning shown by Nd is in the opposite sense to that of La. There appears to be a relationship between the size of the *REE* ions and the probability of uptake *via* the different growth surfaces of the crystal.

Sector lattices

For the monazite studied, the lattice dimensions of each sector type will be slightly different because of the different proportions of *REE* with different ionic sizes that they contain. Therefore each morphological crystal is not single, but can be regarded as being composed of eight individual single-crystal sectors, as four pairs; 011 and 0$\bar{1}\bar{1}$, 0$\bar{1}$1 and 01$\bar{1}$, $\bar{1}$01 and 10$\bar{1}$, 100 and $\bar{1}$00. Although differences in lattice parameters will be small in magnitude, the abrupt change in chemistry and cell size at sector boundaries will probably result in some small angular mismatch between lattice planes in adjacent sectors. In an attempt to calculate what this angular mismatch might be, cell parameters were first calculated for each sector from their chemical compositions and these are included in Table 1. Cell parameters were calculated assuming a linear interpolation between (*REE*)PO_4 end member values (JCPDS data); using the *REE* content alone to calculate relative cell dimensions of these phosphates is valid because Ca, Fe, Sr, Y, Th, U and Si values are either negligible or near-constant for all sectors. Thus calculated, small relative cell differences (if not absolute values) are apparent between the different sectors. Assuming lattice coherency at sector boundaries, the angular mismatch of lattice planes at {$\bar{1}$01}/{011} sector boundaries is calculated to be close to 2° (see Fig. 5 and Table 2.). An angular mismatch of this kind would partly compensate for the differences in lattice sizes and would maximize the coherency of structure at sector boundaries. This explanation is consistent with the small (~2°) angular lattice misorientations observed on precession and Laue photographs of the sector-zoned monazite crystal studied.

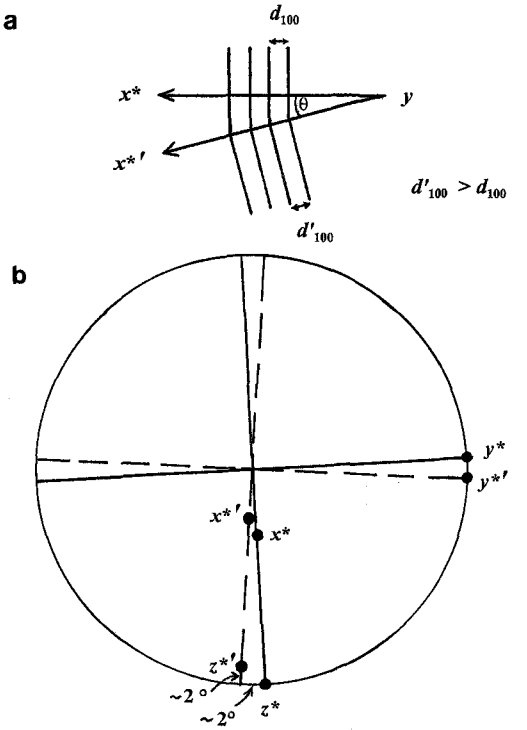

FIG. 5. *a*. Angular mismatch of lattice (for $d'_{100} > d_{100}$) between two sectors to preserve lattice coherency at sector boundary. (*b*) Sketch stereogram representing the relative crystallographic orientations between adjacent 011 and $\bar{1}$01 sectors (Table 2, Fig. 2.).

Interpretation and discussion

Surface structural controls on sector zoning

In sector-zoned crystals the observed differences in chemistry between sectors has been shown to be related to differences in atomic structure on different growth surfaces (e.g. Hollister, 1970; Nakamura, 1973; Dowty, 1976; Reeder and Prosky, 1986; Reeder and Paquette, 1989; Fouke and Reeder, 1992; Rakovan *et al.*, 1997). The concept of a partially-completed structural site, or 'protosite' (a term introduced by Nakamura, 1973) has been used in many of these studies to interpret the formation of sector zoning based on the different geometrical configurations of protosites on different growth surfaces. Crystal surfaces grow primarily by a spiral mechanism (Sunagawa, 1984; Chernov, 1984; Sunagawa, 1987; Pina *et al.*, 1998) whereby atomic units are incorporated predominantly at kink sites in steps that form where a screw dislocation, or other defect, emerges at the surface of a crystal. The step advances laterally by the repeated formation and filling of protosites at edge and kink (corner) site positions. The structural roles and partitioning influence of non-equivalent kink sites with

TABLE 2. Calculated lattice mismatch between sector zones in monazite

Sector	Calculated cell parameters* and lattice spacings (Å)					Calculated angular mismatch of lattice between sectors (degrees)
	a	*b*	*c*	β		
{$\bar{1}$01} (La-low, Nd-high)	6.796	7.022	6.468	103.4	d_{100} = 6.611 | d_{001} = 6.292 | d_{010} = 7.022 |	$\theta_1 = \cos^{-1}(d_{100}/d'_{100}) = 2.4°$ $\theta_2 = \cos^{-1}(d_{001}/d'_{001}) = 2.5°$ $\theta_3 = \cos^{-1}(d_{010}/d'_{010}) = 2.6°$
{011} (La-high , Nd-low)	6.802	7.029	6.474	103.4	d'_{100} = 6.617 | d'_{001} = 6.298 | d'_{010} = 7.029 |	

* cell parameters are calculated from chemical analyses (Table 1), and are average values determined from 20 microprobe analyses from {$\bar{1}$01} sector zones, and 35 analyses from {011} sector zones of the crystal in Fig. 3.

different site sizes and geometries that occur on time-synchronous crystal growth surfaces are now well established (e.g. Staudt *et al.*, 1994, Paquette and Reeder 1995, Rakovan and Reeder, 1996). Depending on factors such as ionic size/charge and speciation in the transport medium, particular cations will be adsorbed onto the surface and attracted to exposed protosites (regions of negative electric potential) with different probabilities of being incorporated in the growing crystal. In studies of differential *REE* uptake during the growth of apatite, Rakovan and Reeder (1994, 1996) and Rakovan *et al.* (1997) conclude that there is an ion-size dependence on the REE^{3+} entering protosites in non-equivalent kink positions. In this study of monazite growth surfaces, we also consider the influence of different kink site geometries on the element uptake and partitioning behaviour of REE^{3+} ions of different size.

In order to investigate the element partitioning behaviour at different growth surfaces in sector zoned monazite, the bulk and surface topologies of the monazite structure need to be examined. Monazite ($P2_1/n$) has a distorted zircon-type structure ($I4_1/amd$). In zircon, Zr atoms are coordinated to eight oxygens of six SiO_4 groups. This cation-anion arrangement is distorted in the monazite structure, such that a seventh anion group (PO_4) is included in the cation coordination sphere. The *REE* ions in monazite occupy a single crystallographic site with point symmetry 1, and are co-ordinated by ten oxygens of the seven nearest-neighbour PO_4 tetrahedral groups. There is a large static disorder in the interatomic *REE*-oxygen distances; bond lengths vary from ~2.4–3Å. During crystal growth, a proportion of *REE* sites at the surface will be only partly constructed. That is to say, some of the PO_4 groups will already be bound to the crystal surface *via* subsurface *REE* ions, but the site cation and further PO_4 units necessary to enclose and capture a *REE* ion will be missing, i.e. protosites will exist on each growth surface. For a spiral growth mechanism, edge and kink protosites will be the ones that predominantly capture and incorporate *REE*. Because of the low site symmetry, the topology of the *REE* site, when partially-constructed, will appear very different in different orientations. In particular, the geometry of the aperture opening to each kink site, as defined by the oxygens of PO_4 units already in place, will depend upon which particular PO_4 groups are missing as governed by the orientation of the kink site in the structural step of the spiral growth plane involved. After adsorption onto the surface, a *REE* ion must eventually pass through the entrance to the kink site in order to take up a stable position within the ligand cage. The site entrance will then be capped by further PO_4 units to complete the co-ordination of the surface site.

In order to visualise the different possible orientations of kink sites on each growth surface, stereopairs of the completed *REE* site in monazite, viewed perpendicular to ($\bar{1}$01), (100) and (011) are shown in Fig. 6(*a*–*h*), using structural parameters taken from Wyckoff (1965). Each diagram (*a*–*h*) shows the same *REE* site, but in different orientations: for the space group symmetry of monazite ($P2_1/n$) two distinct orientations of the *REE* site occur on each of the {$\bar{1}$01} and {100} surfaces respectively, and

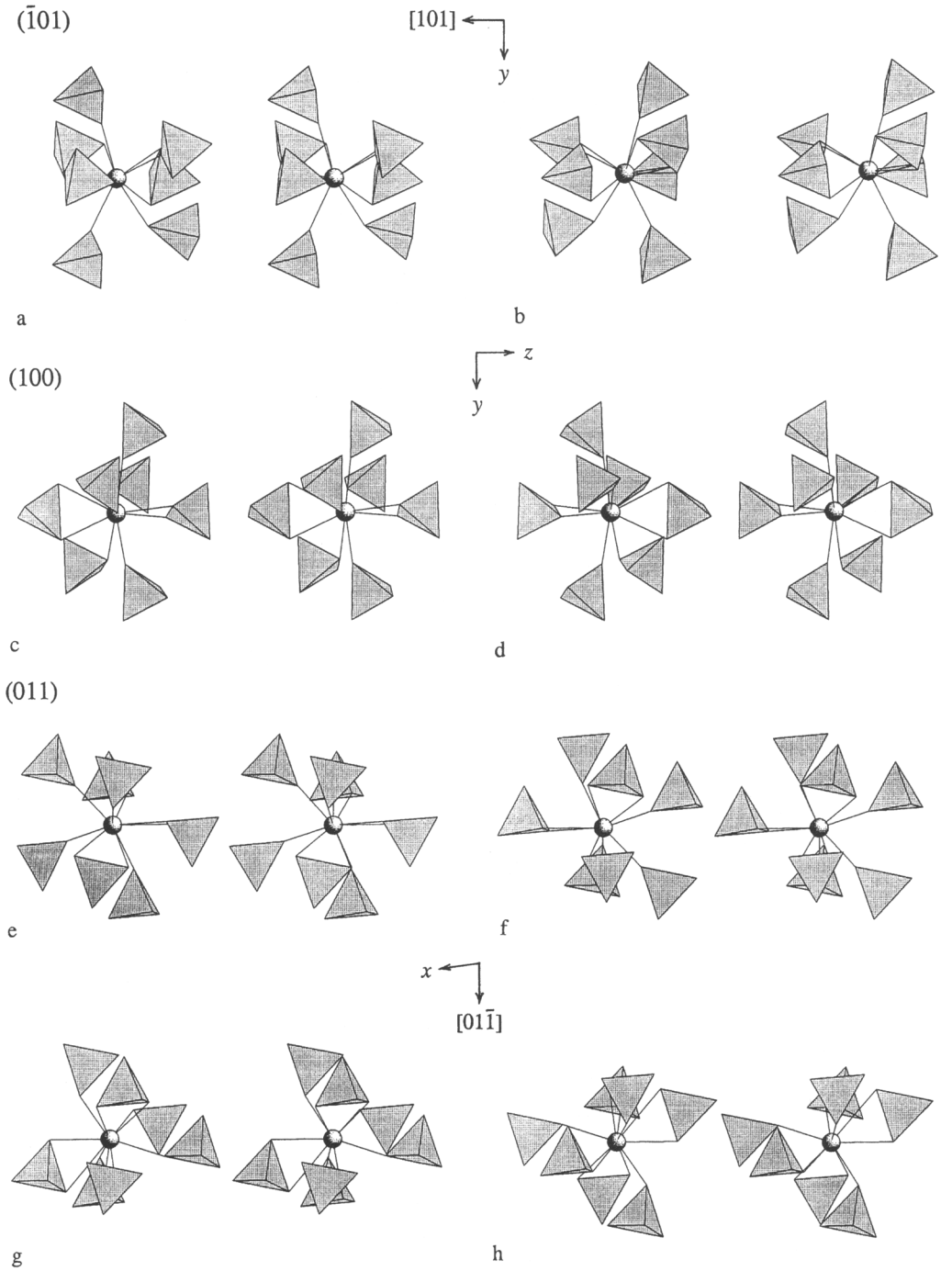

FIG. 6. Stereopairs showing the orientations of the single *REE* site in monazite viewed perpendicular to (1̄01), (100) and (011) growth surfaces. As a result of the crystal symmetry ($P2_1/n$), two distinct orientations of this site occur on {1̄01} (*a*–*b*) and {100} (*c*–*d*), and four on {011} (*e*–*h*).

four distinct orientations occur on the {011} surfaces. The *REE* site is shown as a complete ligand cage formed by PO_4 units, where each tetrahedral PO_4 group can be regarded as a rigid unit because of its high degree of covalent bonding. The plane of the paper represents the plane of the spiral growth step, so different kink site geometries can be appreciated by the 'visual removal' of one or more PO_4 groups to form kink edge steps in different directions. In the stereo-pairs, the PO_4 units appearing closest to the observer are those that form the top of the step, and those that appear furthest away are in the subsurface at the bottom of the step (see Fig. 8). Figure 7 illustrates the *REE* site in monazite as a space-filling representation for oxygen anions of 1.4 Å radius (Shannon, 1976), and indicates which oxygens are 'paired', i.e. belong to the same PO_4 group. Possible kink site geometries can be generated by removal of oxygens from this ligand cage. The absence of one PO_4 group may involve the absence of either one oxygen or two oxygens ('paired') from the coordination sphere. Details of kink sites with one absent PO_4 group are given in Table 3. Examples of possible kink sites are illustrated in Fig. 8, showing that the same kink site geometry can occur on different faces, but will be in a different orientation with respect to the growth step. A particular kink site geometry is likely to incorporate a particular *REE* ion size with similar probability even on morphologically different growth surfaces. However, if equal weighting is given to the existence of all possible kink sites, then the same kink sites occur with different frequencies on different growth surfaces (see Table 3). Kink and edge sites with more than one PO_4 group absent are less likely to discriminate between different sized *REE* ions, because access to the site will not be restricted. However, kink sites with one absent PO_4 group are likely to alter the probability of *REE*-size uptake because their site entrance (gateway) sizes are sufficiently different. An estimate can be made of the maximum size of ion, r_{max}, that could pass through the configuration of oxygen atoms of radius 1.4 Å that define each kink site entrance and these are given in Table 3. Because the kink site gateway size is considered to have an influence on the kinetic behaviour by which cations of different sizes may enter the site, the notion of cation radii is thought appropriate in describing the relative gateway sizes of these different kink sites. From Table 3, it is apparent that for the kink sites listed, their

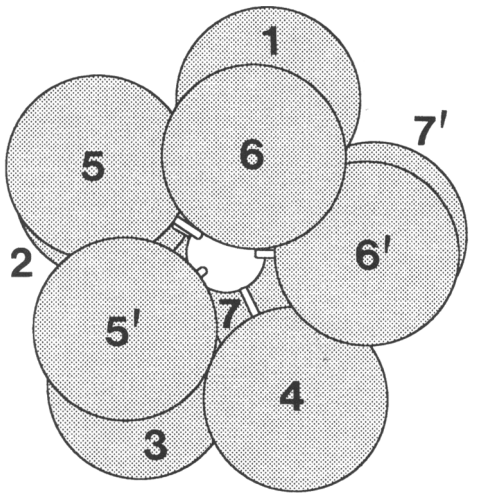

FIG. 7. The *REE* site in monazite illustrated as a space-filling representation with oxygen anions of 1.4 Å radius, shown in the same orientation as Fig. 6*b*. The numbers identifying each oxygen are those used to define kink sites in Table 3. Pairs of oxygen atoms belonging to the same PO_4 group are indicated by 5-5' etc.

measured gateway sizes differ by up to 25% (i.e. from 0.93–1.18 Å). It is also apparent that the kink sites with the smallest gateway dimensions could occur in quite different proportions on ($\bar{1}$01) relative to (011) growth surfaces. The two kink sites (KS3 and KS4) with the smallest gateway sizes are calculated to occur with about doubled frequency on ($\bar{1}$01) relative to (011). In the light of the higher Nd/La ratios observed for the {$\bar{1}$01} sectors relative to {011} sectors, it may be reasonable to assume that the probability of *REE* uptake is altered in proportion to the frequency of occurrence of KS3 and KS4 on these two growth surfaces, with these two kink sites discriminating in favour of the smaller-sized *REE*. It is instructive to consider the different proportions of small-gateway kink sites (KS3 + KS4) calculated to be present on the different growth surfaces of monazite. The ratio, [proportion of small-gateway kink sites (KS3 + KS4) on ($\bar{1}$01)]/[proportion of small-gateway kink sites (KS3 + KS4) on (011)] = 1.69 (calculated from data in Table 3). It is interesting to note that, from the observed chemical data (Table 1), the ratio, [Nd/La in {$\bar{1}$01} sectors]/[Nd/La in {011} sectors] = 1.74, suggesting that the change in

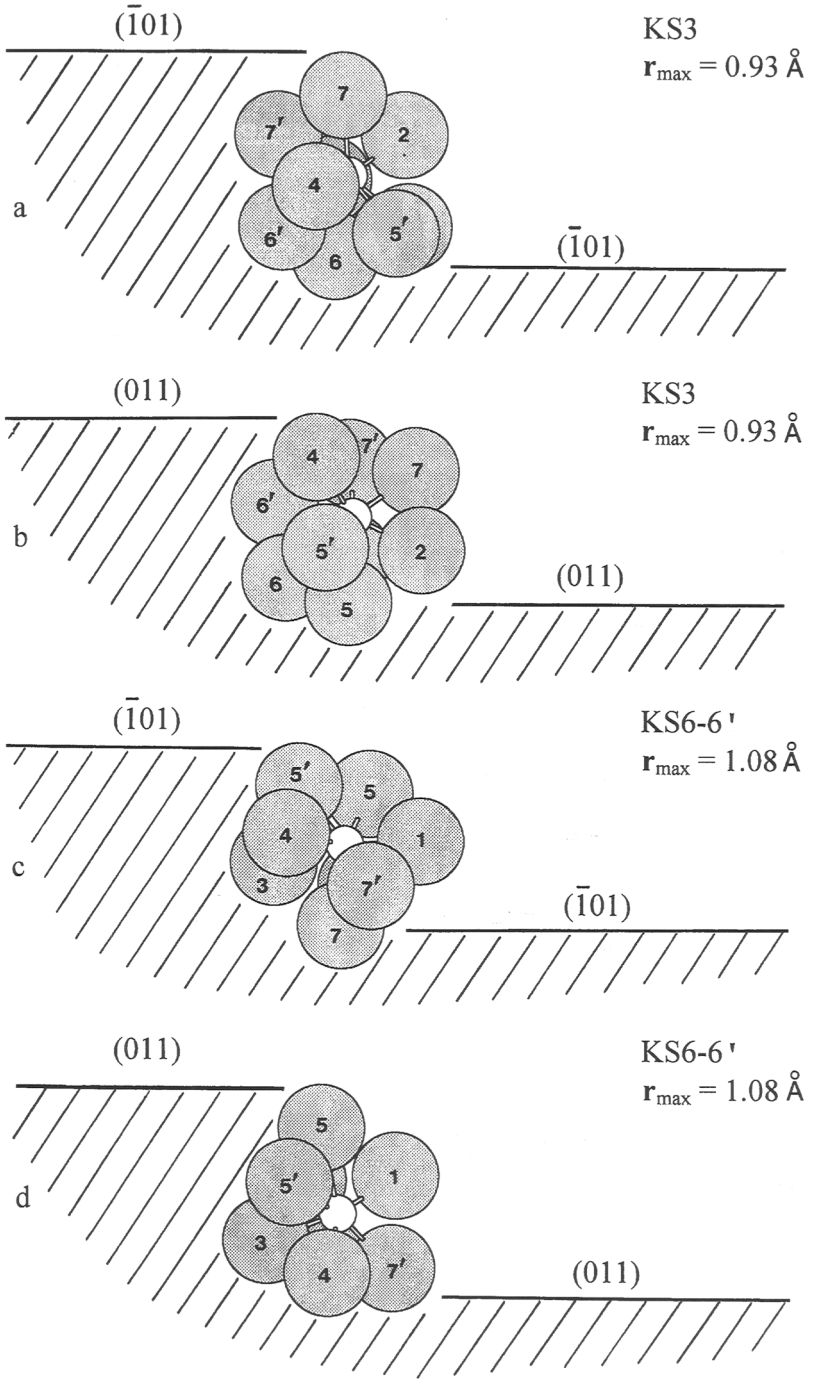

FIG. 8. Two possible kink sites (KS3 and KS6-6') showing their different orientations at edge steps on (1̄01) and (011) growth surfaces. Kink site (KS) types and r_{max} values (relating to the size of the entrance to the site) are given in Table 3. Oxygen atoms are identified by the same numbers used in Fig. 7.

TABLE 3. Comparison of kink sites on different growth faces of monazite

Kink site (KS) type*	r_{max}**	Relative numbers of possible kink sites (KS) for each distinct orientation (*a*–*h*, in Fig. 6) of the *REE* site on different growth faces. ***													
		($\bar{1}$01)				(100)				(011)					
		a	b	tot.	%	c	d	tot.	%	e	f	g	h	tot.	%
KS1 (O1)	1.10	1	1	2	20.0	1	1	2	16.7	1	0	1	0	2	11.8
KS2 (O4)	1.05	1	0	1	10.0	0	1	1	8.3	1	0	1	1	3	17.6
KS3 (O3)	0.93	1	1	2	20.0	1	1	2	16.7	0	1	0	1	2	11.8
KS4 (O2)	0.95	1	1	2	20.0	1	1	2	16.7	0	1	0	1	2	11.8
KS5-5′(O2-O1)	1.18	0	1	1	10.0	1	1	2	16.7	1	0	0	1	2	11.8
KS6-6′(O3-O2)	1.08	0	1	1	10.0	1	0	1	8.3	1	1	1	1	4	23.5
KS7-7′(O3-O4)	1.03	1	0	1	10.0	1	1	2	16.7	0	1	1	0	2	11.8

* Each kink site type is based on one absent PO_4 group. Absent oxygen(s) are given in parentheses.
** Maximum radius cation that could enter kink site, based on oxygens of 1.4 Å radii that define the site entrances.
*** A zero entry signifies that the kink site does not occur in the orientation specified, because the PO_4 group required to be absent is already present below the surface.

uptake probability of small *REE* may be linked to the occurrence frequency of the smaller-gateway kink sites. However, this correlation should be viewed only qualitatively, because it is not known how the occurrence of the larger-gateway kink site types (present on all surfaces) might affect the uptake probability in favour of the larger La ion.

The calculated relative proportions of the different kink sites are quite similar for ($\bar{1}$01) and (100) morphological growth surfaces, and the observed *REE* compositions of {$\bar{1}$01} and {100} sectors are also very similar. A subtle, but measurable, characteristic of {100} sector chemistry is the presence of a higher level of Sr (Table 1) relative to the other sectors. It should be noted that the kink site (KS5-5') with the largest gateway is calculated to occur with highest frequency on (100) relative to ($\bar{1}$01) and (011) surfaces. The accommodation of a relatively large cation, such as Sr^{2+} (with a considerably larger ionic radius than La^{3+} for a given coordination), may occur with slightly higher probability if large-gateway kink sites are present. A local charge-balancing proton may also be involved in this incorporation.

Because of the thermal motion of the oxygen atoms together with possible structural relaxation effects at crystal surfaces, absolute values for r_{max} only offer an approximate model for element incorporation at the crystal surface. However, assuming similar degrees of distortion and thermal motion at each growth surface, the relative sizes of the kink site gateways on each surface will alter the kinetics of element uptake and the probabilities with which *REE* ions of a particular size will be incorporated into each surface. If the thermal motions of the oxygens are anisotropic and are surface dependent, then the chemical partitioning kinetic behaviour between sectors might also be temperature dependent.

Crystal morphology and growth rates of sectors

The relative sizes of the gateway entrances to edge and kink sites on the monazite crystal surfaces may also influence the relative growth rates in different directions. The flattened morphology, with large {$\bar{1}$01} faces shown by all the monazites in these rocks, indicates that growth rates were faster in directions perpendicular to {011} and {100} faces relative to those perpendicular to {$\bar{1}$01}. The same conclusion can be drawn from observing the relative thickness of the late-stage overgrowth rims that crystallized on the different sector surfaces (see Fig. 3). The anisotropy in surface protosite characteristics is likely to be responsible for the observed growth rates. A higher proportion of the larger-gateway kink sites is calculated to occur on {011} surfaces, relative to those on {$\bar{1}$01}, and these sites may present less of a kinetic barrier to the incorporation of the larger *REE* ions. For this reason, in the presence of a growth medium highly enriched in the light *REE* (La and Ce), kinetic partitioning of these larger ions may be achieved more easily on {011} growth faces

relative to {$\bar{1}01$} faces. This analysis is consistent with the observed monazite growth shape.

Watson and Liang (1995) and Watson (1996) have proposed a model for the development of sector zoning that depends on the competition between growth rate and lattice diffusion within the near-surface layer. In this model, surface enrichment of a particular element, resulting from chemical equilibrium between the growth medium and the types of atomic sites present at the crystal surface, will be preserved if the growth rate is sufficiently fast to bury the enriched layer before the element can escape to the surface by diffusion. Thus, sector zoning is unavoidable in crystals that exhibit selective enrichment on certain growth surfaces. Watson (1996) also points out that sector zoned crystals can deviate substantially from homogeneous equilibrium as a result of the kinetic controls that influence anisotropic element uptake at different surfaces. Rakovan and Reeder (1994) have discussed ideas on non-equilibrium partitioning and suggest that there is no unique value of K_D that describes the actual partitioning for a given mineral-fluid system, but rather, propose that the partitioning system should be viewed as a set of effective K_D values that differ for structurally distinct regions on crystal surfaces.

Anisotropy in chemical uptake by the different faces of a growing crystal is likely to be present in most crystals to a greater or lesser degree. There are, perhaps, four reasons why this particular type of zoning has not been more commonly observed in monazite: (1) The effect is very subtle and not easy to correlate with optical observations. (2) In some cases, subsequent diffusion in the bulk crystal may have obliterated original sector zoning, for example at high temperature during prograde metamorphic recrystallization, or in high temperature igneous crystallization. (3) Major changes in fluid chemistry may produce a strong concentric zoning overprint. (4) Thorium, commonly present in monazites in amounts up to 31 wt.% ThO_2 (Overstreet, 1967; Förster and Harlov, 1999) may modify the monazite structure, influence morphology and cause additional complications in zoning patterns. The Th-free monazite crystals we have studied here show relatively uncomplicated sector zoning and have a morphology flattened on {$\bar{1}01$} with significant development of {011} and only small development of {100}. It is interesting to note that (the more common) Th-bearing monazites have a different morphology; they are flattened on {100}, have smaller {$\bar{1}01$} faces, and do not develop the {011} form. It is likely that the presence of Th influences the morphology generated, thus causing different sector growth forms to develop with the result that sector uptake probabilities are distinctly different to those that develop when Th is absent from the growth medium.

Sector zoning may go unnoticed in many crystals, especially if the chemical differences between growth surfaces are minimal because the differences in the probabilities of uptake are small. Differences in uptake for a particular element will generally be greater for sites of low symmetry and high distortion, and will be related to the ability of the whole structure to form particular growth faces. The ability of particular ions (including trace ions) to alter the morphology of a growing crystal is well known (e.g. Kostov, 1968; Wilken, 1977; Titiloye *et al.*, 1993; Staudt *et al.*, 1994; Reeder and Paquette, 1989; Reeder and Prosky, 1986). So the physicochemical state of the fluid/melt will contribute significantly in the first instance to the development of particular growth forms, and could thereby determine the subsequent element uptake behaviour of each sector surface. Energetically favourable surfaces will therefore be stabilized by particular ions, thereby introducing a particular growth form that will continue to incorporate the favoured ion on that surface, until some limiting physicochemical change occurs. The overall morphology, and subsequent anisotropic element uptake behaviour by sectors, will have been controlled by a combination of different key ions.

Conclusions

The sector zoning of *REE* in monazite from the Kangankunde carbonatite has been interpreted as a surface uptake behaviour related to *REE* ionic size. The probability of *REE* uptake by different sector faces is likely to have been governed by the size of the *REE* ion and by the variations in orientation and geometry of the partially-constructed acceptor sites on each growth surface. The *REE* ion-exchange reactions will have been constantly operative at each growth surface and different *REE* site occupancies have been preserved within each sector; these are evidence of the time-synchronous, anisotropic element uptake behaviour of monazite growth surfaces.

Acknowledgements

The authors wish to thank Terry Williams and John Spratt of the Natural History Museum for help with electron microprobe analyses, and the reviewers whose comments led to an improvement of this paper.

References

Burt, D.M. (1989) Compositional and phase relations among rare earth elements. In *Geochemistry and mineralogy of rare earth elements* (B.R. Lipin and G.A. McKay, eds). Reviews in Mineralogy, **21**, Mineralogical Society of America, pp. 259–307.

Chernov, A.A. (1984) *Modern Crystallography III.* Springer-Verlag, Berlin.

Clark, A.M. (1993) Hey's Mineral Index. Chapman & Hall, London, 851 pp.

Dowty, E. (1976) Crystal structure and crystal growth: II. Sector zoning in minerals. *Amer. Mineral.*, **61**, 460–9.

Dowty, E. (1980) Computing and drawing crystal shapes. *Amer. Mineral.*, **65**, 465–71.

Förster, H.-J. and Harlov, D.E. (1999) Monazite(Ce)-huttonite solid solutions in granulite-facies metabasites from the Ivrea-Verbano Zone, Italy. *Mineral. Mag.*, **63**, 587–94.

Fouke, B.W. and Reeder R.J. (1992) Surface structural controls on dolomite composition. *Geochim. Cosmochim Acta*, **56**, 4015–24.

Garson, M.S. (1966) Carbonatites in Malawi. In *Carbonatites* (O.F. Tuttle and J. Gittins, eds). Wiley, London, pp. 33–71.

Garson, M.S. and Campbell-Smith, W. (1965) *Carbonatite and agglomeratic vents in the Western Shire Valley.* Geological Survey of Malawi, Memoir no. **3**, Government Press, Zomba, Malawi.

Hollister, L.S. (1970) Origin, mechanism, and consequences of compositional sector-zoning in staurolite. *Mineral. Mag.*, **55**, 742–66.

Holt, D.N. (1965) *The Kangankunde Hill rare earth prospect. Results of an economic investigation.* Malawi Ministry of Natural Resouces, Geological Survey Department, Bulletin **20**, Government Press, Zomba, 130 p.

Kapustin, Yu. L. (1980) *Mineralogy of carbonatites.* Amerind Publishing, New Delhi, 259 p. (Translated from Russian: *Mineralogiya Karbonatitov*, 1971) Nauka Publishers, Moscow.

Kostov, I. (1968) *Mineralogy.* Oliver and Boyd.

Le Bas, M.J. (1989) Diversification of carbonatite. In *Carbonatites: genesis and evolution* (K. Bell, ed.). Unwin Hyman, London, pp. 428–47.

Nakamura, Y. (1973) Origin of sector-zoning of igneous clinopyroxenes. *Amer. Mineral.*, **58**, 986–90.

Ni, Y., Hughes, J.M. and Mariano, A.N. (1995) The crystal chemistry of monazite and xenotime structures. *Amer. Mineral.*, **80**, 21–6.

Overstreet, W.C. (1967) The geologic occurrence of monazite. *USGS Prof. paper*, **530**, 1–327.

Paquette, J. and Reeder, R.J. (1995) Relationship between surface structure, growth mechanism, and trace element incorporation in calcite. *Geochim. Cosmochim. Acta*, **59**, 735–49.

Pina, C.M., Becker, U., Risthaus, P., Bosbach, D. and Putnis, A. (1998) Molecular-scale mechanisms of crystal growth in barite. *Nature*, **395**, 483–6.

Rakovan, J. and Reeder, R.J. (1994) Differential incorporation of trace elements and dissymmetrization in apatite: The role of surface structure during growth. *Amer. Mineral.*, **79**, 892–903.

Rakovan, J. and Reeder, R.J. (1996) Intracrystalline rare earth element distributions in apatite: Surface structural influences on incorporation during growth. *Geochim. Cosmochim. Acta*, **60**, 4435–45.

Rakovan, J., McDaniel, D.K. and Reeder, R.J. (1997) Use of surface-controlled REE sectoral zoning in apatite from Llallagua, Bolivia, to determine a single-crystal Sm-Nd age. *Earth Planet. Sci. Lett.*, **146**, 329–36.

Reeder, R.J. and Paquette, J. (1989) Sector zoning in natural and synthetic calcites. *Sedim. Geol.*, **65**, 239–47.

Reeder, R.J. and Prosky , J.L. (1986) Compositional sector zoning in dolomite. *J. Sed. Petrol.*, **56**, 237–47.

Roberts, W.L., Campbell, T.J. and Rapp Jr., G.R. (1990) *Encyclopedia of minerals.* 2nd edition, Van Nostrand Reinhold Company, New York, 979 p.

Shannon, R.D. (1976) Revised effective ionic radii and systematic studies of interatomic distances in halides and chalcogenides. *Acta Crystallogr.*, **A32**, 751–67.

Staudt, W.J., Reeder, R.J. and Schoonen, M.A.A. (1994) Surface structural controls on compositional zoning of SO_4^{2-} and SeO_4^{2-} in synthetic calcite single crystals. *Geochim. Cosmochim. Acta*, **58**, 2087–98.

Sunagawa, I. (1984) Growth of crystals in nature. In *Materials Science of the Earth's Interior* (I. Sunagawa, ed.). Terra Scientific, Tokyo, pp. 63–105.

Sunagawa, I. (1987) Morphology of minerals. In *Morphology of Crystals* (I. Sunagawa, ed.). Terra Scientific, Tokyo, pp. 509–87.

Titiloye, J.O., Parker, S.C. and Mann, S. (1993) Atomistic simulation of calcite surfaces and the influence of growth additives on their morphology. *J. Cryst. Growth*, **131**, 533–45.

Wall, F. and Mariano, A.N. (1996) Rare earth minerals in carbonatites: a discussion centred on the Kangankunde Carbonatite, Malawi. In *Rare earth*

minerals: chemistry, origin and ore deposits (A.P. Jones, F. Wall and T.C. Williams, eds). Mineralogical Society Series, **7**, Chapman & Hall, London, pp. 193–225.

Watson, E.B. (1996) Surface enrichment and trace-element uptake during crystal growth. *Geochim. Cosmochim. Acta*, **60**, 5013–20.

Watson, E.B. and Liang, Y. (1995) A simple model for sector zoning in slowly grown crystals: Implications for growth rate and lattice diffusion, with emphasis on accessory minerals in crustal rocks. *Amer. Mineral.*, **80**, 1179–87.

Wilken, G. (1977) Surface features of synthetic silicate garnets. *J. Cryst. Growth*, **40**, 165–8.

Woolley, A.R. (1991) The Chilwa alkaline igneous province of Malawi: a review. In *Magmatism in Extensional Structural Settings. The Phanerozoic African Plate* (A.B. Kampunzu and R.T. Lubala, eds). Springer-Verlag, Berlin, pp. 377–409.

Wyckoff, R.W.G. (1965) *Crystal Structures*, 2nd ed., Vol 3. Interscience, New York.

[*Manuscript received 20 January 1999: revised 21 August 1999*]